THE ASTROPHYSICAL JOURNAL, 361:197–206, 1990 September 20

AN ATMOSPHERIC ANALYSIS OF THE CARBON-RICH WHITE DWARF G35–26[1]

PETER THEJLL, HARRY L. SHIPMAN, JAMES MACDONALD, AND W. M. MACFARLAND
Department of Physics and Astronomy, University of Delaware

ABSTRACT

We present the first detailed spectral analysis of the DQ white dwarf G35–26 (Gr 469, WD 0203+207). Based on the published spectra, we determine that the dominant atmospheric constituent is He and that the temperature lies between 11,000 K and 14,000 K, the hydrogen abundance is between $n(\mathrm{H})/n(\mathrm{tot}) = 0.01$ and 0.005, and the carbon abundance is close to $n(\mathrm{C})/n(\mathrm{tot}) = 0.03$. The breadth of H$\beta$ and Hγ and the virtual absence of Hδ suggests a high gravity—between $\log(g) = 9$ and $\log(g) = 9.5$. If this gravity is correct, it gives G35–26 the highest mass (1.2–1.33 $M_\odot$) yet observed for a single white dwarf, if it is placed on the zero-temperature Hamada-Salpeter (H-S) relation. O+Ne+Mg white dwarfs in the range 1.2–1.37 $M_\odot$ are predicted by theory, and G35–26 might be the first such object discovered, providing unique study opportunities. Given an H-S radius, the distance is between 33 and 69 pc. Based on the abundances that we find, there is no inconsistency in assuming that the hydrogen was accreted from the interstellar medium and that the carbon is due to dredge-up, since accretion of the observed amounts of C would leave detectable amounts of N, O, and Ca in the photosphere, whereas accretion of N, O, and Ca along with the H would not. At the moment no further progress is likely in the analysis of G35–26 until better spectra are made and an accurate parallax is measured.

Subject headings: stars: abundances — stars: individual (G35–26) — stars: white dwarfs

I. INTRODUCTION

G35–26 was long thought to be a DA with a strong magnetic field (for example, Greenstein 1978; Hintzen and Jensen 1979). This was based on the appearance of the apparently Zeeman split Balmer lines. However, since the star is faint (V is about 17.4), it was hard to identify the features in the available spectra. Liebert (1983) obtained better spectra and showed that the magnetic field is no stronger than 5×10^5 G, and that the previously supposed Zeeman components are carbon lines. G35–26 was thus one of the first white dwarfs to show both hydrogen and carbon lines. Another example is the star G227–5 (Wegner and Koester 1985). A number of degenerate stars show carbon lines, and at lower temperatures the molecular bands of C_2.

The model for dredge-up (Koester, Weidemann, and Zeidler 1982; Wegner and Yackovich 1983) of the diffusion-distributed carbon tail in cool helium-rich white dwarfs is by now the well-established explanation for the presence of carbon in these stars. A detailed investigation (Pelletier *et al.* 1986) of the interaction of the surface convection zone and the diffusion tail of the interior carbon distribution can explain the observed carbon abundance/T_{eff} relation. The theory has also shown how the total He mass (m_{He}) will influence the phenomenon. When m_{He} is below 10^{-6} $M_\odot$, mixing of the helium and the carbon will occur—if this happened the atmosphere would no longer be helium-dominated, with traces of carbon, but would show larger amounts of carbon. The literature now contains many analyses of white dwarfs that show carbon features, and each star adds support to the dredge-up theory. Although G35–26 (Gr 469, WD 0203+207) shows carbon features in the spectrum, it is not a simple example of a conventional DB with carbon since it shows hydrogen lines.

In this paper we present the first detailed atmospheric analysis of G35–26 based on the published spectra and on helium-rich, homogeneous, blanketed, LTE models, containing carbon, hydrogen, and small amounts of N, O, and Ca, and on the assumption that G35–26 is a single star. We fit the observed spectra against the model spectra and determine T_{eff}, $\log(g)$, and the abundance of H, He, C, and upper limits on N, O, and Ca. We also derive the mass and the zero temperature Hamada-Salpeter radius, the distance, the parallax, and the tangential velocity. Finally, we discuss possible uncertainties in our findings, as well as possible evolutionary implications.

II. THE PHYSICS INPUT

Liebert (1983) pointed out that in G35–26 the Balmer lines drop in strength very quickly: Hβ is much stronger than Hγ, and Hδ is virtually absent. High gravity or some other broadening mechanism can achieve this. Van der Waals broadening of the Balmer lines by neutral helium is important at the temperature of G35–26—estimated (Liebert 1983) at about 14,000 K—so we include van der Waals broadening of the hydrogen lines, due to neutral helium and neutral carbon, in our atmospheric code, ATLAS (Kurucz 1970).

Carbon I lines are modeled by Voigt profiles with Stark parameters and oscillator strengths taken from Fawcett (1987), Goly, Rakotoarijmy, and Weniger (1983), Victor and Escalante (1988), Wiese, Smith, and Gennon (1966), and Wiese and Konjevic (1982). In cases where many published and different values of atomic parameters are available, we take averages with a preference for later works. Carbon I UV lines have an important influence on the atmospheric structure because of the blanketing effect and were therefore included. We also included some C II lines. The Stark parameters for C II lines are somewhat hard to come by—Griem (1974) lists values for only a few C II lines, so we used the method of scaling the Stark parameters in a isoelectronic sequence (Dimitrijevic and Popovic 1989) and found as many C II Stark parameters as possible: optical C II lines that blend with C I lines at 4267 Å, the 3589 Å line and two UV lines at 687 Å and 858 Å. At the

1 Send reprint requests to Harry L. Shipman.

TABLE 1

ADOPTED VALUES FOR VARIOUS LINES USED IN THIS WORK

λ(Å)	gf[a]	χ (eV)	w (Å)[c]	Ionization Potential (eV)
		Carbon I Line Data		
4268.99.....	0.437×10^{-2}	0.768×10^{1}	0.395	0.113×10^{2}
4371.33.....	0.832×10^{-2}	0.768×10^{1}	0.315	0.113×10^{2}
4762.41.....	0.631×10^{-2}	0.748×10^{1}	0.124	0.113×10^{2}
4762.41.....	0.525×10^{-2}	0.748×10^{1}	0.124	0.113×10^{2}
4766.62.....	0.398×10^{-2}	0.748×10^{1}	0.120	0.113×10^{2}
4770.00.....	0.525×10^{-2}	0.748×10^{1}	0.130	0.113×10^{2}
4771.72.....	0.200×10^{-1}	0.749×10^{1}	0.110	0.113×10^{2}
4775.87.....	0.631×10^{-2}	0.749×10^{1}	0.100	0.113×10^{2}
4812.84.....	0.102×10^{-2}	0.748×10^{1}	0.110	0.113×10^{2}
4817.33.....	0.295×10^{-2}	0.748×10^{1}	0.140	0.113×10^{2}
4826.73.....	0.490×10^{-2}	0.749×10^{1}	0.120	0.113×10^{2}
4932.00.....	0.166×10^{-1}	0.768×10^{1}	0.250	0.113×10^{2}
5039.05.....	0.245×10^{-2}	0.748×10^{1}	0.104	0.113×10^{2}
5039.05.....	0.550×10^{-2}	0.748×10^{1}	0.104	0.113×10^{2}
5041.66.....	0.102×10^{-1}	0.749×10^{1}	0.104	0.113×10^{2}
5044.00.....	0.186×10^{-2}	0.748×10^{1}	0.104	0.113×10^{2}
5049.60.....	0.186×10^{-2}	0.749×10^{1}	0.104	0.113×10^{2}
5052.12.....	0.324×10^{-1}	0.768×10^{1}	0.180	0.113×10^{2}
5054.50.....	0.126×10^{-3}	0.749×10^{1}	0.104	0.113×10^{2}
5380.24.....	0.209×10^{-1}	0.768×10^{1}	0.130	0.113×10^{2}
1657.20.....	0.151×10^{1}	0.400×10^{-2}	0.174×10^{-2}	0.113×10^{2}
1930.93.....	0.407	0.126×10^{1}	0.221×10^{-2}	0.113×10^{2}
2478.56.....	0.930×10^{-1}	0.268×10^{1}	0.361×10^{-2}	0.113×10^{2}
1279.25.....	0.190×10^{-1}	0.500×10^{-2}	0.321×10^{-2}	0.113×10^{2}
1277.50.....	0.575	0.400×10^{-2}	0.299×10^{-2}	0.113×10^{2}
1261.30.....	0.263	0.400×10^{-2}	0.495×10^{-2}	0.113×10^{2}
1481.77.....	0.550×10^{-1}	0.126×10^{1}	0.341×10^{-2}	0.113×10^{2}
1463.33.....	0.468	0.126×10^{1}	0.387×10^{-2}	0.113×10^{2}
1459.05.....	0.350×10^{-1}	0.126×10^{1}	0.391×10^{-2}	0.113×10^{2}
1751.90.....	0.120	0.268×10^{1}	0.562×10^{-2}	0.113×10^{2}
1280.40.....	0.182	0.400×10^{-2}	0.734×10^{-2}	0.113×10^{2}
1467.45.....	0.450×10^{-1}	0.126×10^{1}	0.729×10^{-2}	0.113×10^{2}
1764.00.....	0.300×10^{-2}	0.268×10^{1}	0.105×10^{-1}	0.113×10^{2}
1364.14.....	0.600×10^{-2}	0.126×10^{1}	0.313×10^{-1}	0.113×10^{2}
6587.75.....	0.460×10^{-1}	0.853×10^{1}	0.115×10^{1}	0.113×10^{2}
		Carbon II Line Data		
3589.30.....	0.214×10^{1}	0.225×10^{2}	0.458	0.244×10^{2}
4267.27.....	0.537×10^{1}	0.209×10^{2}	0.997	0.244×10^{2}
4267.02.....	0.380×10^{1}	0.209×10^{2}	0.997	0.244×10^{2}
4267.20.....	0.269	0.209×10^{2}	0.997	0.244×10^{2}
858.41.....	0.275	0.530×10^{-2}	0.824×10^{-2}	0.244×10^{2}
687.25.....	0.155×10^{1}	0.530×10^{-2}	0.214×10^{-2}	0.244×10^{2}
		Nitrogen I Line Data		
4256.30.....	0.107	0.103×10^{2}	0.707×10^{-1}	0.145×10^{2}
4222.00.....	0.234	0.103×10^{2}	0.745×10^{-1}	0.145×10^{2}
4146.30.....	0.260×10^{-1}	0.103×10^{2}	0.806×10^{-1}	0.145×10^{2}
4928.20.....	0.170×10^{-1}	0.107×10^{2}	0.102	0.145×10^{2}
5200.50.....	0.560×10^{-1}	0.116×10^{2}	0.239×10^{1}	0.145×10^{2}
1199.90.....	0.141×10^{1}	0.000	0.690×10^{-3}	0.145×10^{2}
1493.30.....	0.110×10^{1}	0.238×10^{1}	0.125×10^{-2}	0.145×10^{2}
1743.60.....	0.550	0.358×10^{1}	0.170×10^{-2}	0.145×10^{2}
1243.30.....	0.107×10^{1}	0.238×10^{1}	0.791×10^{-3}	0.145×10^{2}
1411.94.....	0.155	0.358×10^{1}	0.102×10^{-2}	0.145×10^{2}
1167.90.....	0.347	0.238×10^{1}	0.279×10^{-2}	0.145×10^{2}
1164.00.....	0.955×10^{-1}	0.238×10^{1}	0.306×10^{-2}	0.145×10^{2}
1319.50.....	0.204	0.358×10^{1}	0.325×10^{-2}	0.145×10^{2}
1316.29.....	0.380×10^{-2}	0.358×10^{1}	0.345×10^{-2}	0.145×10^{2}
1310.70.....	0.331	0.358×10^{1}	0.388×10^{-2}	0.145×10^{2}
1176.90.....	0.138	0.238×10^{1}	0.500×10^{-2}	0.145×10^{2}
1327.00.....	0.316×10^{-1}	0.358×10^{1}	0.636×10^{-2}	0.145×10^{2}
1100.70.....	0.363×10^{-1}	0.238×10^{1}	0.108×10^{-1}	0.145×10^{2}
		Oxygen I Line Data		
3947.29.....	0.110×10^{-1}	0.914×10^{1}	0.626×10^{-1}	0.136×10^{2}
4368.00.....	0.170×10^{-1}	0.952×10^{1}	0.802×10^{-1}	0.136×10^{2}

TABLE 1—*Continued*

λ(Å)	gf[a]	χ (eV)	w (Å)[c]	Ionization Potential (eV)
		Oxygen I Line Data		
6157.30.....	0.998	0.107×10^2	0.116×10^1	0.136×10^2
6455.00.....	0.222	0.107×10^2	0.490	0.136×10^2
5330.00.....	0.209	0.107×10^2	0.292×10^1	0.136×10^2
5436.10.....	0.680×10^{-1}	0.107×10^2	0.100×10^1	0.136×10^2
6046.40.....	0.380×10^{-1}	0.110×10^2	0.131×10^1	0.136×10^2
1303.50.....	0.288	0.967×10^{-2}	0.821×10^{-3}	0.136×10^2
989.46.....	0.501	0.967×10^{-2}	0.423×10^{-3}	0.136×10^2
1152.16.....	0.447	0.197×10^1	0.646×10^{-3}	0.136×10^2
1026.60.....	0.912×10^{-1}	0.967×10^{-2}	0.244×10^{-2}	0.136×10^2
		Calcium I Line Data		
4226.00.....	0.175×10^1	0.293×10^1	0.630×10^{-2}	0.611×10^1
		Calcium II Line Data		
3945.00.....	0.138×10^1	0.313×10^1	0.149	0.119×10^2

[a] Product of the statistical weight and the oscillator strength for the multiplet.
[b] Excitation potential.
[c] Stark width, defined at an electron density of 10^{16} cm^{-3} and at 10,000 K.

temperatures we are interested in, the optical C II lines are weak. We list the atomic parameters for the included lines in Table 1. There are no obvious lines present at the wavelengths for N I, O I, or Ca I or II in the spectra of G35–26, so we can, by modeling these lines, at most derive upper limits on the N, O, and Ca abundances. These lines were modeled by Voigt profiles, the atomic data being taken from the usual sources: Griem (1974), Moore (1971), and Wiese, Smith, and Glennon (1966). The He I line at 4471 Å is modeled by the Barnard, Cooper, and Shamey (1969) theory. Other He I lines are included as well, although the ones visible in the optical are all weaker than 4471. The resonance lines of He I are normally of great importance when the flux at 500–600 Å is large—this is not the case in G35–26 where $T_{\rm eff}$ is lower, and the opacity below 1500 Å, due to carbon, is very large.

Since some of the carbon lines are close to the Balmer lines, it is important to calculate the spectra in a way that allows for line blending. The atmosphere program that we use, ATLAS, is based on imposing flux constancy, and the models were converged in hydrostatic equilibrium, allowing for line blanketing and convection. Bound-free, free-free, and scattering opacities from electrons and all relevant elements and ionization stages are included. Iteration was continued until the flux errors were small, or until the temperature structure did not change significantly.

Because ATLAS uses a Λ-iteration to correct the temperature near the surface it can be inefficient when there is strong scattering in these layers. The iterations will seemingly converge in the sense that the temperature corrections are small but the corrections "never" really disappear—you would need a very large number of iterations to truly converge the procedure. The Λ-operator is linear in its action so we used the second-order acceleration scheme due to Ng (1974), as described by Auer (1987). It will in some cases accelerate the convergence.

A grid of models covering 10,000, 12,000, and 14,000 K, log (g) = 8, 8.5, 9, and 9.5, and n(He)/n(H) of 200, 100, and 50 was calculated. Carbon was varied between 100 and 200 times solar abundance. N, O, and Ca were scaled experimentally until their optical lines were invisible at the level of typical noise in G35–26. The theoretical spectra were convolved with a Gaussian profile of the same resolution as the observed spectra—4 Å in the case of the detailed spectrum of Hβ by Liebert, and 7 Å in the case of his "blue" spectrum. The IDS spectrum of Hintzen and Jensen apparently has a resolution of 7 Å, too.

a) The Importance of C_2 *Opacity*

At the temperatures we are interested in here (lower than 14,000 K) the opacity due to molecules of C_2 can be important, depending on the exact temperature and the amount of carbon. The initial temperature estimates for G35–26—14,000 K—made it questionable whether C_2 opacity would be important or not. Even if there are no signs of the Swan bands in the spectra of G35–26, we wanted to be sure that we had a good description of the radiative transfer since the strength of the Balmer lines, which blend with the Swan bands at cooler temperatures, are decisive in the derivation of the stellar parameters. Short of incorporating molecular opacities in ATLAS, we performed a rough scaling of published spectra with C_2 bands (Yackovich 1982). We compared the density of C_2 molecules—calculated using the partition function data in Yackovich (1982)—in the models that best fit G35–26, to the C_2 density in a 10,000 K/log (g) = 8 model of similar C abundance. Yackovich presents a spectrum with molecular opacity of such a model, and in it the Swan bands are prominent. In the models that describe G35–26 best, the density of C_2 is down by a factor of at least 10^{-3} so it is not likely that Swan bands would be visible if we included them in our models. See Figure 1. We therefore did not model C_2 opacity in this work.

b) Continuum C *Opacities*

Since wide-band spectral information is available for G35–26, we wanted to model the slope of the continuum as accurately as possible and therefore included opacity due to C^- and Rayleigh scattering from C I. In ATLAS there is already opacity for H_2^+, H^-, and He^-, along with Rayleigh scattering opacities for H_2 and He. We used the combined bound-free and free-free cross section for C^-, as presented by Myerscough and McDowell (1966). There are newer calcu-

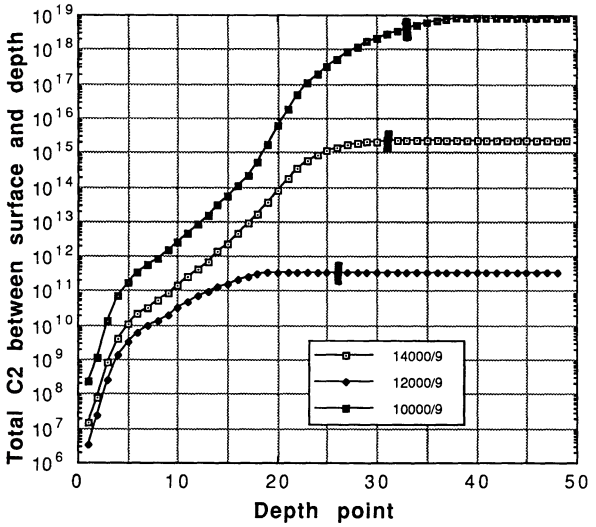

FIG. 1.—Line-of-sight sum of the molecular carbon density in three models at 10,000, 12,000, and 14,000 K. Rosseland optical depth 1 is indicated on the curves, and we see that between the 10,000 and 12,000 K model, the total amount of molecular carbon drops by three or four orders of magnitude at the place where molecular features could be expected to form. The molecular densities were calculated using partition function data from Yackovich (1982).

lations of the cross section—for instance, Bell, Hibbert, and Berrington (1988) give free-free cross sections that are somewhat different from the older values. However, the form it is presented in is not as convenient as that in Myerscough and McDowell so we gauged the importance of the differences by introducing a scaling factor and converging two models with different settings of the factor. There was no significant influence on the fluxes. The C I Rayleigh scattering included is that due to Tarafdar and Vardya (1969).

c) *Van der Waals Broadening*

Finally we consider van der Waals broadening of hydrogen by neutral carbon atoms. Van der Waals broadening of hydrogen by helium, along with the Stark broadening, is included in ATLAS in a hydrogen-line profile routine that is due to Deane Peterson, but we also wished to consider van der Waals broadening of hydrogen by neutral carbon since the strengths of the hydrogen lines are pivotal to the conclusions of this paper. We used a simple scaling relation to estimate the importance of the C/H interaction, comparing it to the He/H interaction. We follow essentially Gray (1976) and use a simplified picture of the interaction in which the phase shifts induced by only those encounters with an impact parameter less than a critical value are included. This procedure gives a width that scales as

$$\left(\frac{v_{\rm He}}{v_{\rm H}}\right)^{3/5}\left[\frac{C_6({\rm He})}{C_6({\rm H})}\right]^{2/5} N({\rm He\ I}) \qquad (1)$$

for the He/H interaction. Here $v_{\rm He}$ is the velocity of the helium-atoms, N(He I) is the density, by numbers, of helium atoms and C_6 is the van der Waals interaction constant. To make the coding easy we introduce the C/H interaction as a scaling factor on the helium density:

$$\left(\frac{v_{\rm He}}{v_{\rm H}}\right)^{2/3}\left[\frac{C_6({\rm He})}{C_6({\rm H})}\right]^{2/5} N({\rm He\ I}) + \left(\frac{v_{\rm C}}{v_{\rm H}}\right)^{3/5}\left[\frac{C_6({\rm C})}{C_6({\rm H})}\right]^{2/5} N({\rm C\ I}) \qquad (2)$$

$$= f \times \left(\frac{v_{\rm He}}{v_{\rm H}}\right)^{3/5}\left[\frac{C_6({\rm He})}{C_6({\rm H})}\right]^{2/5} N({\rm He\ I})\,. \qquad (3)$$

This gives

$$f = 1 + \left(\frac{v_{\rm C}}{v_{\rm He}}\right)^{3/5} \times \left[\frac{C_6({\rm C})}{C_6({\rm He})}\right]^{2/5} \frac{N({\rm C\ I})}{N({\rm He\ I})}\,. \qquad (4)$$

The velocities are calculated from energy equipartitioning, and the ratio of the van der Waals interaction constants can be estimated from the ratio of the polarizabilities, to which the interaction strength is proportional. We get

$$f = 1 + 0.72 \times 2.36 \times \frac{N({\rm C\ I})}{N({\rm He\ I})} = 1 + 1.7 \times \frac{N({\rm C\ I})}{N({\rm He\ I})}\,, \qquad (5)$$

where the ratio of the densities will be calculated in LTE and thus depends only on the temperature and the abundances. Hence one atom of carbon replaces nearly two helium atoms in the van der Waals broadening effect on H. Below we will consider whether carbon broadening of H lines can mimic the broadening due to high gravity without making C I lines too strong.

We do not include van der Waals broadening of C I lines.

III. OBSERVATIONAL DATA

The V magnitude for G35–26 is 17.39 mag (McCook and Sion 1987). The best parallax available through 1988 is 0".0060 ± 0".0054 (C. C. Dahn 1990, private communication), and the proper motion is 0".34 yr^{-1} (Greenstein 1978). The present parallax has a high error, but improvements will be hard to achieve because the field of view of the CCD used at the US Naval Observatory is not sufficiently wide to allow observation of the parallax of G35–26, and photographic techniques have to be used. The spectra we use were observed by Hintzen and Jensen (1979) and Liebert (1983). Multichannel data was observed by Greenstein (1978) and can be used to limit the effective temperature.

We wished to perform the fitting of the spectra by using the equivalent widths of the spectral lines. Because the observed spectra are noisy (Fig. 2), it is hard to measure the equivalent widths. The observed spectra also contain some long-wavelength undulations that make it hard to tell the extent of line wings. Some of the small carbon lines are not much different in strength or shape from the noise spikes, so, for these

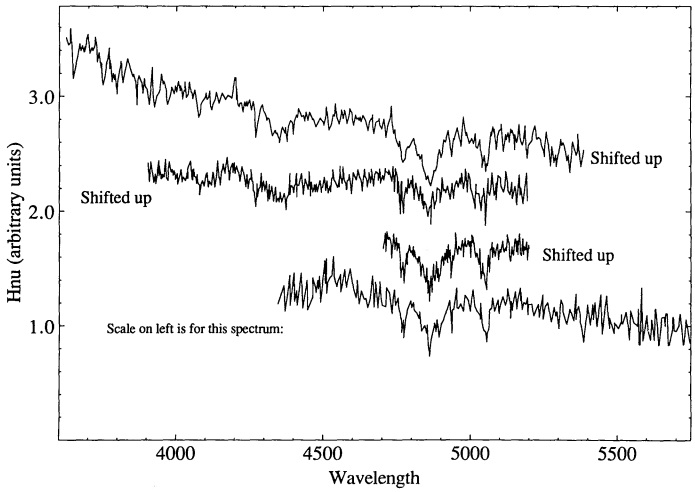

FIG. 2.—The published spectra of G35–26. They have all been normalized to the same flux at 4700 Å and then separated to allow comparison of spectral features. Notice the weakness of Hγ and the virtual absence of higher order Balmer lines.

lines, we can at best measure order-of-magnitude equivalent widths. Due to the blending of C and H-lines we chose to measure the widths using the shoulders of the H lines as the continuum. For consistency we measure the theoretical widths in this fashion as well. It is particularly hard to measure an equivalent width of the γ and δ Balmer lines. We set wide limits and integrated the combined H and C profiles and then subtracted the individually measured C line widths. There is barely any sign of He I—there may be a slight dip at 4471. We derived an upper limit on w_{4471} which can be used to set an upper limit to $T_{\rm eff}$. The averaged equivalent widths for G35–26 are given in Table 2.

IV. FITTING $T_{\rm eff}$, log (g) AND ABUNDANCES

The high frequency noise at the 5%–10% level in the spectra, and the "ripples" or "bumps," along with an unrealistic continuum slope, makes it difficult to correctly estimate the significance of the best fit between models and observations, and we decline to offer a quality estimate; we merely report where the best fit is.

We calculated the equivalent width for all lines of interest, along with rough estimates of the error on each, in the observed spectra and in the models, and calculated a χ^2 statistic for each model and drew contour plots of it for each temperature and carbon abundance, as a function of He/H ratio and log (g). We likewise fitted the Hβ profile against the model profiles, after convolving the model profiles by the observational resolution (4 Å) and got a χ^2 for each model. The results are shown in Figures 3 and 4. Generally the best fit is such that log (g) is at least 9.0, He/H is somewhere between 50 and 200, while the carbon abundance is between 100 and 200 times the solar abundance. By detailed study of how the strengths of the C I lines vary with C abundance we constrain n(C)/n(tot) to lie between 100 and 200 times the solar value (solar value = $10^{-3.49}$) with a *strong* upper limit at 400. While increased C mimics the effect that He has on the broadening of H—and the "disappearance" of Hδ (see Fig. 5)—there is no doubt that at the average $T_{\rm eff}$, log (g) (= 13,000 K, 9.25) a value of n(C)/n(tot) above 400 times the solar value produces C I lines that are much stronger than the ones observed (Fig. 6).

We use the multichannel data to limit the temperature. Neither 10,000 K nor 14,000 K gives a satisfactory fit; the 12,000 K model has the best fit, and 11,000 and 13,000 K probably form the limits on $T_{\rm eff}$. The temperature 14,000 K

TABLE 2

MEASURED, AVERAGED EQUIVALENT WIDTHS FOR G35–26 AND THE EQUIVALENT WIDTHS FROM THE BEST-FITTING MODEL

Line	$W \pm$ Estimated Error (Å)	W (theory)
Hδ	$4 + 1/-3$	5
C I 4268	$4 + 0.5/-1$	1
Hγ	18 ± 7	18
C I 4371	1 ± 0.5	1
He I 4471	<3	~0
C I 4771	5 ± 1	4
Hβ	25 ± 9	31
C I 4932	1 ± 0.5	1
C I 5050	9 ± 2	5

NOTE.—Widths were measured in the same way in observed spectra and in the 13,000 K, log (g) = 9.25, n(H)/n(tot) = 0.0096, n(C)/n(tot) = 0.03 model.

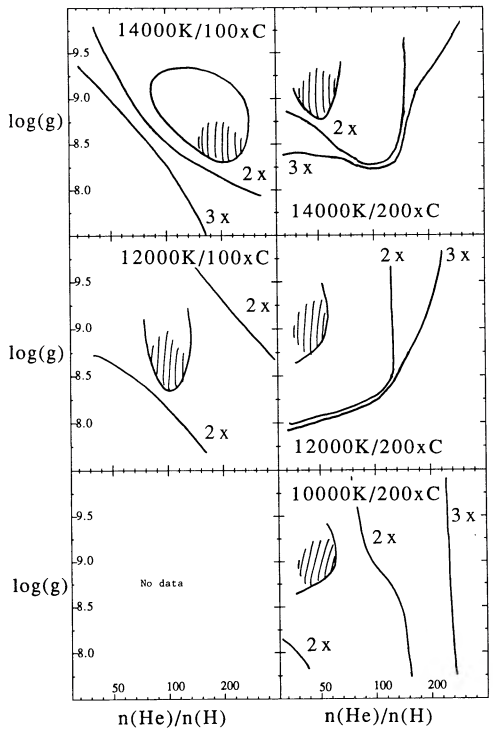

FIG. 3.—The χ^2 fit for G35–26 using equivalent widths. Each panel is for a specific effective temperature and carbon abundance. The hatched regions show where the best fit is located in each panel. The contours show where the χ^2 has increased by a certain amount.

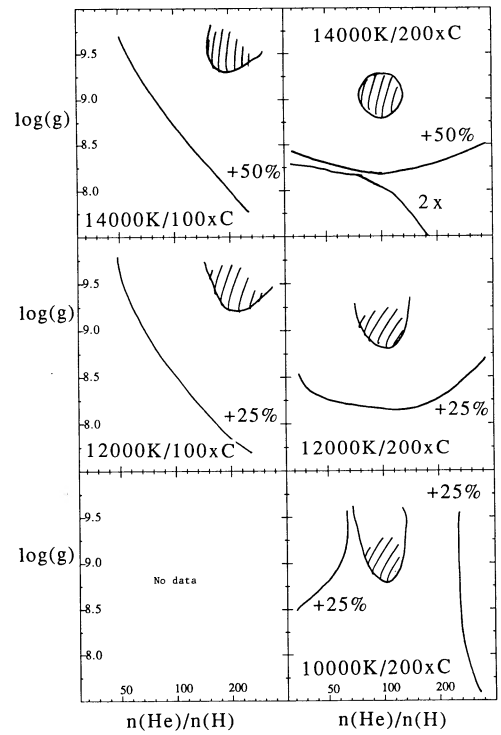

FIG. 4.—Like Fig. 3 but for the χ^2 fit of the best line profile available—the detailed Hβ profile by Liebert.

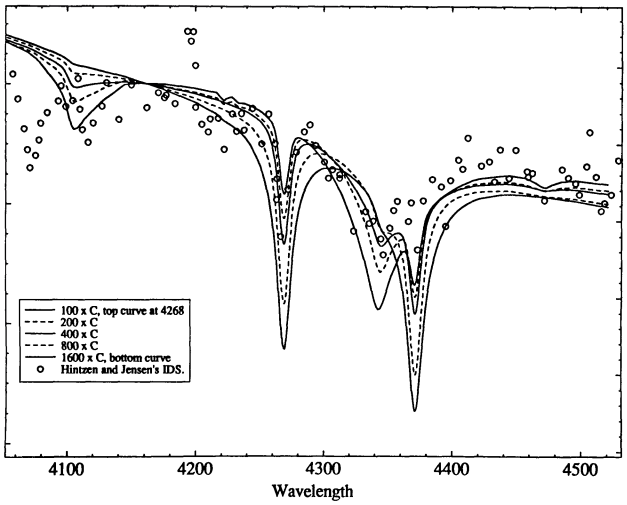

FIG. 5.—Models with various carbon abundances and Hintzen and Jensen's IDS spectrum. 13,000 K, log (g) = 9.25, n(H)/n(tot) = 0.0096). Reading from the weakest to the strongest C I feature—at 4268 Å, for instance—the carbon abundances are 100, 200, 400, 800, and 1600 times the solar value. Any abundance above 400 times the solar value is ruled out. Note how increased carbon mimics the effect of increasing the helium abundance in weakening the Hδ line—however, values of n(C)/n(tot) greater than 400 times the solar value, are strictly ruled out by the strength of the C I lines. Only part of the flux scale is shown.

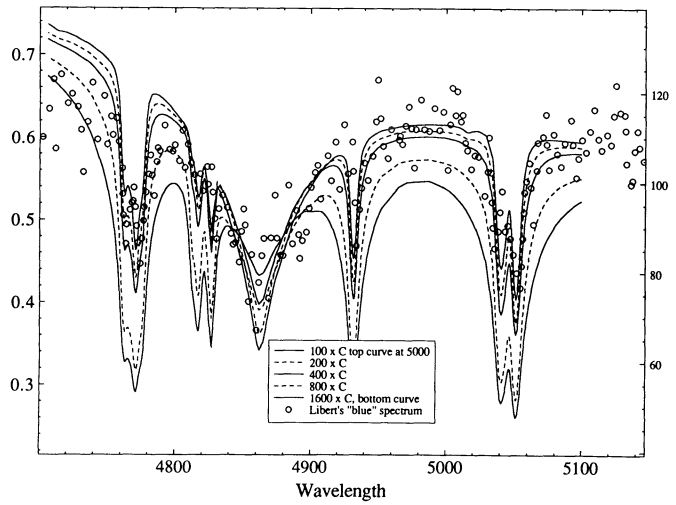

FIG. 6.—Like Fig. 5 but for the Hβ line. Again n(C)/n(tot) greater than 400 times the solar value is ruled out by the strength of the C I features.

is furthermore ruled out by the weakness of He I 4471. See Figure 7.

The absence of molecular C_2 features in G35–26 set a lower limit on the temperature. We estimate, from studies of a DQ star (G47–18) modeled at 10,000 K, with similar C abundance (Yackovich 1982), that the temperature of G35–26 could be a little bit above 10,000 K. We base this estimate on the line-of-sight sum of C_2 in models at different effective temperatures. See Figure 1. At 11,000 K, the C_2 line-of-sight abundance is so much smaller than at 10,000 K that C_2 features would hardly be visible above the noise.

The equivalent widths of the observable lines, measured in the best fitting model, are listed in Table 2. The fit is not perfect, but with the exception of C I at 4268 Å and to a lesser extent that at 5050 Å, the observed and predicted widths agree within the estimated errors.

Based on the above analysis of the available data, we feel justified in saying that G35–26 has a helium-dominated atmosphere, has a $T_{\rm eff}$ between 11,000 K and 14,000 K, log (g) between 9 and 9.5, n(H)/n(tot) between 0.01 and 0.005, and n(C)/n(tot) = 0.03. The values of n(N)/n(tot), n(O)/n(tot), and n(Ca)/n(tot) cannot be above 1 times the solar value, a limit set by the noise in the spectra. The N, O, and Ca lines used are those between 3900 and about 5500 Å.

The large gravity is controversial, especially taking the low quality of the data into consideration, and we wish to point out that while the best fit, given the present data and models, is at high gravity, the final judgment must be made when better data are at hand. We will in what follows discuss the conse-

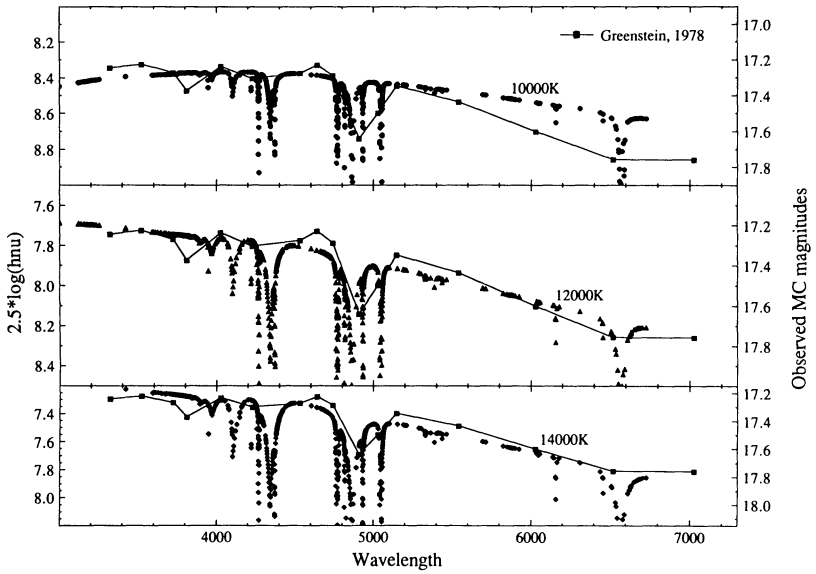

FIG. 7.—Multichannel data from Greenstein (1978) compared to models at 12,000 K and 14,000 K, log (g) = 9, He to H = 200, and n(C)/n(tot) = 100 times solar abundance. The slope of the 12,000 K model, in the blue end of the spectra, fits the data better than does that of the 14,000 K model.

TABLE 3

RADIUS-DISTANCE RATIO OF G35–26

$T_{\rm eff}$/log (g)	R/D	D (pc)	π (H-S)	d (H-S) (pc)
12,000/9.....	2.3×10^{-12}	$52\sqrt{M/M_\odot}$	0".019	56
14,000/9.....	1.9×10^{-12}	$64\sqrt{M/M_\odot}$	0.014	69
12,000/9.5.....	2.3×10^{-12}	$29\sqrt{M/M_\odot}$	0.030	33
14,000/9.5.....	1.9×10^{-12}	$38\sqrt{M/M_\odot}$	0.024	41

NOTE.—π (H-S) and d (H-S) are the parallax and the distance if G35–26 is on the zero-temperature Hamada-Salpeter mass-radius relation for Mg/C. D follows from eq. 6 and $g = GM/R^2$. A measured parallax in the range from 0".015 to 0".03 with a 25% error or less would confirm the gravity we find from the present spectra.

quences of a large gravity, with the knowledge that log (g) may change later.

V. ANALYSIS

a) *Radius-to-Distance Ratio*

We can derive the ratio of the radius of G35–26 to its distance by comparing the observed flux f_V at the V magnitude frequency and the Eddington flux calculated for the best fitting models. The observed flux is 4.15×10^{-27} ergs cm^{-2} s^{-1} Hz^{-1}. Using this flux and the Eddington fluxes from ATLAS, and the relation

$$4\pi H_\nu R^2 = f_V D^2 , \quad (6)$$

we get the results given in Table 3.

The gravities that follow if the Hamada-Salpeter mass-radius relation is used, along with the ratio R/D in Table 3 and the measured parallax and its errors, are log $g(\pi) = 8.1$, log $g(\pi + \sigma) = 8.8$, log $g(\pi + 2\sigma) = 9.0$ and log $g(\pi + 3\sigma) = 9.4$. We see that the gravity range indicated by the spectral fit corresponds to 2 and 3 σ deviations of the parallax from its mean. To confirm our high mass a parallax in the range 0".014–0".03 with an error of no more than 25% or so must be measured. Conversely, the present parallax of 0".006 $\pm$ 0".0054 needs to have its error reduced to the 20%–30% level to rule out a gravity of log (g) = 9.0 at more than the 3 σ level.

b) *The Possible Mass*

On Figure 8 we show a portion of the mass-radius diagram with the Hamada-Salpeter relations for Fe, Mg, and C compositions along with lines of constant gravity. Sirius B fails to fall on the zero temperature relation (Kidder, Holberg, and Wesemael 1988), by a significant amount, for several reasons (see Thejll and Shipman 1986 for a more thorough discussion); the temperature is not zero—this influences the volume of the atmosphere and hence the radius of the star; the molecular weight of the atmosphere must be taken into account; and the role of residual nuclear buring is not clear for high-mass stars—Koester and Schönberner (1986) have looked at this question, but only for stars of lower mass. Rotation and magnetic fields also alter the mass-radius relation. G35–26 could thus also be expected to fall above the zero temperature relation, but to a smaller extent due to the lower temperature and higher gravity. For gravities between log (g) = 9 and log (g) = 9.5, we see that, for C + O and O + Ne + Mg interiors, masses between 1.2 and 1.33 solar masses, and radii between 0.003 and 0.005 solar radii, are indicated.

The large value of the tangential velocity of 263 km s^{-1} reported by Greenstein (1978) follows from assuming

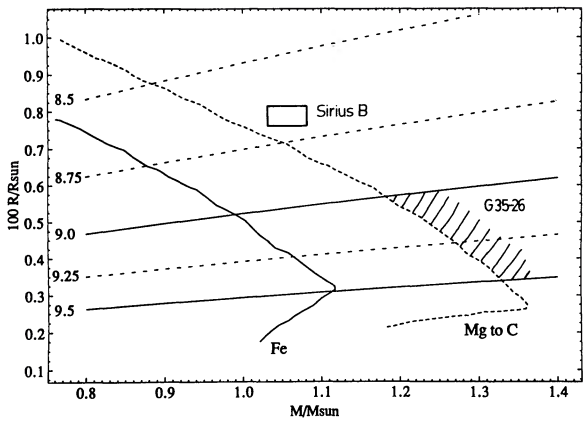

FIG. 8.—Mass radius diagram. The lines marked Fe and Mg to C are the Hamada-Salpeter relations. The line marked Mg to C represents an average of the relations expected for elements from C through O and Ne to Mg, based on the atomic weight. The three white dwarfs Sirius B, Eri 40B, and Stein 2051, for which independent masses and radii exist, are the only stars that at the moment formally support the mass-radius relation. The numbered lines are lines of log constant gravity. G35–26 is somewhere between the 9.0 and 9.5 lines, on the basis of the present analysis.

log (g) = 8.0. Using higher gravities decreases the distance and lowers the velocity. For the range of distances that follow from the spectral gravity fit we get the range of velocities 72 to 95 km s^{-1}—this is higher than the average for the majority of white dwarfs ($\approx$50 km s) (Sion *et al.* 1988) as is typical for DQ stars. The very large tangential velocity corresponding to log (g) = 8—263 km s^{-1}—is an indirect argument against a low gravity. A measurement of the Doppler shift of the lines could help settle this problem.

VI. THE CARBON ABUNDANCE AND CONVECTIVE DREDGE-UP

The derived carbon abundance is near n(C)/n(tot) = 0.03. Models for the pollution of helium-rich white dwarf atmospheres by convective dredge-up of carbon have been studied by Vauclair and Fontaine (1979), Fontaine *et al.* (1984), and Pelletier *et al.* (1986). Pelletier *et al.* find that the observed relationship between carbon abundance and effective temperature is that expected from the evolution of a 0.6 $M_\odot$ CO white dwarf with a 2×10^{-4} $M_\odot$ helium envelope. Although the carbon concentration for G35–26 fits in well with the observed n(C)/n(He)–$T_{\rm eff}$ relation, the surface gravity of G35–26 may well be significantly higher than that of a 0.6 $M_\odot$ white dwarf and the results of Pelletier *et al.* (1986) cannot then be directly applied to G35–26. Instead, we have calculated stratified envelope models of mixtures of helium and carbon. The composition profile is determined from the balance between forces due to gravity, partial pressure gradients, and induced electric fields. In addition, mixing in convection zones is treated as a diffusion process. Further details of the technique used for constructing the models can be found in MacDonald and Vennes (1990). In Figure 9 C/He ratios are plotted as a function of effective temperature for different total helium masses for white dwarfs of mass 0.6 $M_\odot$ and 1.2 $M_\odot$. In general, for 0.6 $M_\odot$, our results are in agreement with the results of Pelletier *et al.* (1986).

The top of the convection zone in both the stratified envelope models and the homogeneous atmosphere models is at a Rosseland optical depth of $\approx$0.4. Hence we can make the assumption that the abundance ratios found from the best-fitting homogeneous atmosphere model for G35–26 are repre-

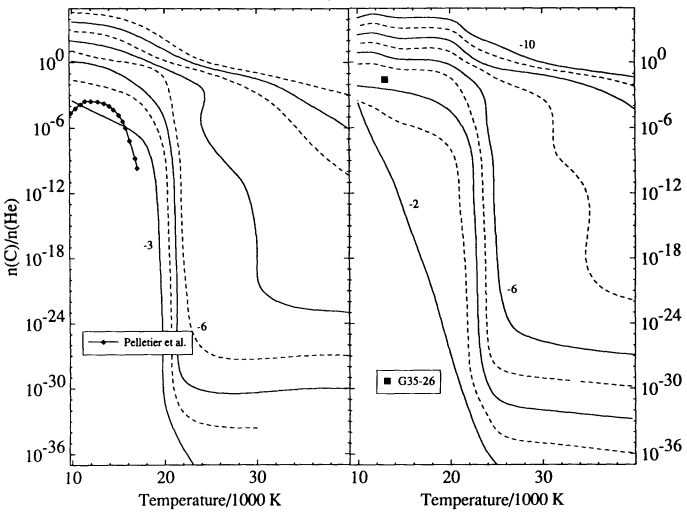

FIG. 9.—In the left panel, predicted n(C)/n(He) at Rosseland photosphere for a 0.6 $M_\odot$ WD, as a function of total helium mass (m_{He}) and effective temperature (T_{eff}). The curve labels are log ($m_{He}/M_\odot$). The data of Pelletier *et al.* for log ($m_{He}/M_\odot$) = −3.7 are superposed. For log ($m_{He}/M_\odot$) ≥ −6, it can be seen that there is a critical T_{eff} where the composition changes from helium-dominated to carbon-enriched. For lower m_{He} the tendency is to be carbon-rich at all temperatures. The right-hand panel is for a 1.2 $M_\odot$ WD. The position of G35–26 is indicated.

sentative of the abundance ratios at a Rosseland optical depth of unity in the stratified envelope. For the composition parameters of G35–26 and mass 1.2 $M_\odot$, we find a helium layer mass of 5×10^{-5} $M_\odot$. In addition, stratified envelope calculations, in which the diffusive equilibrium equations are solved, for mixtures of hydrogen, helium and carbon, give a hydrogen mass of 2–5 $\times 10^{-12}$ $M_\odot$ and a helium mass of 3×10^{-5} $M_\odot$. Much of the hydrogen is mixed in the surface convection zone of mass $\approx 10^{-9}$ $M_\odot$.

The mass of helium found here for G35–26 can be compared to the minimum helium layer mass necessary to sustain nuclear burning by the triple-alpha reaction on a CO core. For 1.2 $M_\odot$ Kawai, Saio, and Nomoto (1988) find, for pure helium envelopes, a minimum helium layer mass of about 10^{-4} $M_\odot$. Near the end of the asymptotic giant branch phase of the pre–white dwarf evolution the helium envelope may contain up to 20% carbon due to convective dredge up (see, e.g., Iben 1984) and the molecular weight will be higher than for pure helium. This results in a higher temperature in the burning shell for given helium mass and hence the total helium mass when nuclear reactions cease will be less than for the pure helium case. Thus, there is no obvious inconsistency between the helium mass found from carbon dredge-up models for G35–26 and the helium layer mass that may be expected from stellar evolution models.

VII. DISCUSSION

We will now discuss some possibilities and problems surrounding the present analysis of G35–26—we do not mean this discussion to be exhaustive and refer the reader to discussions of other aspects of G35–26 in Liebert (1983).

The present analysis is based on spectra and photometric data of rather low quality—has the quality of the data biased our analysis? Most importantly, could the gravity determinations be wrong? The gravity is determined by the smallness of Hγ and the virtual absence of higher order Balmer lines. The spectra are noisy, but lines with equivalent widths of a few angstroms can still be reliably detected—the predicted equivalent widths for Hδ and higher order lines is tens of Å, not close to 1, at gravities 8 and 8.5. Only at log (g) = 9 and 9.5 do they become small enough that the fit, given the noise, is acceptable. We have two independent spectra that verify the smallness of the high-order Balmer lines. While low hydrogen abundances may seem a way to fit G35–26 to log (g) = 8 models, simultaneous fits of the Balmer β, γ, and δ lines are impossible, with the present models.

Could our treatment of line-broadening be inadequate? We have included van der Waals broadening due to neutral helium and carbon in our hydrogen line-broadening code. Other "wide" sources of opacity—like molecular bands—might depress the continuum and make the higher order Balmer lines weak, but we do not see any traces of the strongest Swan band around Hβ. We see no reason to believe in appreciable molecular opacity for the additional reason that we can calculate molecular densities and they are much lower than the C_2 density in the models where molecular bands are evident. We have included appropriate sources of continuous opacity like bound-free and free-free opacity in C^- and Rayleigh scattering due to C I. We have therefore included the most important ways in which the high-order Balmer lines can be made small or very broad due to opacity effects. A detailed treatment of van der Waals broadening due to C I would be attractive but is not likely to add anything substantial to the analysis at the moment, particularly as the gravity fit is not driven by the C I lines.

The models we have used to fit the spectra against are all homogeneous models. If the atmosphere of G35–26 is stratified, the possibility arises that the weak high-order Balmer lines owe their weakness to the stratification. The cross section for lines in the Balmer series decreases as you go toward higher order lines; this means that the higher order lines, like Hγ and Hδ, typically are formed deeper in the photosphere than Hβ. In a stratified atmosphere there would be less hydrogen present at depth and therefore the high-order lines would be weakened. However, our models are all convective up to a Rosseland mean optical depth of about 0.4—close to the point where the lines form. Since convection would remove stratification, and since convective overshoot which is a realistic modification of "ordinary" convection theories would further weaken the stratification, we do not believe in a stratified photosphere for G35–26. Furthermore, the core of any line is formed nearer the surface of the photosphere than are the wings, so each line formed in a stratified photosphere will tend to have a core that is stronger, relative to the wings than would be the case in a homogeneous model. We see by this qualitative argument that higher order Balmer line wings would be weakened—G35–26 has weak high-order Balmer lines, but they are certainly not narrow and thus we doubt the existence of stratification. It is, however, necessary to perform a quantitative analysis of the possibility and also to investigate the influence of alternative convection theories. In the present work we use a convection theory similar to ML1 in all respects except that the mixing length has been set to 1.5.

The high mass that follows from this gravity determination is not ruled out by current stellar evolution theory. Nomoto (1984) describes the possibility that single white dwarfs with O + Ne + Mg cores form from progenitors with masses in the range 8 $M_\odot$ to some value less than 10 $M_\odot$. Such white dwarfs should have masses in the range 1.2–1.37 $M_\odot$. If G35–26 really

TABLE 4

OBSERVED ELEMENTAL ABUNDANCES IN G35–26 COMPARED TO THE SOLAR ABUNDANCES

Element	$n(x)/n(\mathrm{tot})$	$\frac{[n(x)/n(\mathrm{tot})]_{G35-26}}{[n(x)/n(\mathrm{tot})]_{\odot}}$
H	0.005–0.01	$\sim 10^{-2}$
C	0.03	$\sim 10^{2}$
He	0.97	~ 12
N	$<10^{-4}$	<1
O	$<10^{-3}$	<1
Ca	$<10^{-6}$	<1

NOTE.—Abundances relative to the total particle density have been calculated from the abundances given by Allen 1973.

has the high mass we think it has, it would be the first example of such a O + Ne + Mg single white dwarf ever discovered. Evolution of the surface, and interior, chemical abundances can be expected to be entirely different for this object type. As far as we know, there are no detailed investigations of the evolution, or indeed even composition, of the photosphere of an object like this.

Can the composition (see Table 4) of G35–26 be explained by accretion theories? It is not in contradiction with the measured abundances of H, C, N, O, and Ca to explain the appearance of G35–26 in the following manner: The carbon is present due to dredge-up and the hydrogen is due to accretion. The carbon could almost certainly *not* have been accreted since considerable amounts of N, O, and Ca then also would be expected. The hydrogen *could* be accreted since the small amounts of O, N, and Ca that would accompany the hydrogen would not be visible in the present spectra.

In conclusion, G35–26 seems to be a high-mass DB white dwarf that has accreted hydrogen and is undergoing convective dredge-up of interior carbon. Evolutionary theory has predicted the existence of massive O + Ne + Mg WD's, but there are no predictions, as yet, of the atmospheric constitution or chemical evolution of these objects. Other possibilities exist that might explain the peculiar spectrum, and they must be exhaustively investigated, before we can be sure that G35–26 is the first star of this kind to be observed. G35–26 is not just interesting in itself but also provides a test bed for accretion and dredge-up theories and for stellar evolution theories. *If* G35–26 is what we think it is, a O + Ne + Mg WD, then an explanation of the elemental abundances will lend strong support to the successful theory in that G35–26 widens the range of stellar parameters available for study. With a good parallax, G35–26 could also add a data point on an entirely new section of the mass-radius relation. The mass-radius relation for white dwarfs has so far only been strictly verified for three objects; Sirius B, 40 Eri B, and Stein 2051. No one seriously doubts the relation but a data point at the stability "knee" would be of great value in the continuing analysis of Chandrasekhar's original idea.

At the moment, better observational data is needed. The spectra are too noisy to yield further insight. A significantly better optical spectrum should be obtainable with a 4 m telescope in one night of observation and would not only provide a clearer picture of the relative strengths of the Balmer lines, and thus the gravity, but would also allow determination of the Doppler shift and hence give information on the spatial motion of G35–26, which would help in understanding its kinematics and evolution. Stricter limits on the abundances of heavy elements (particularly through the Ca H + K line) could be placed and would further restrict the possible evolutionary scenarios. If ultraviolet spectra could be obtained, from the ground (3200–4000 Å) or from space (1100 Å and up), it would be possible to analyze the very strong resonance lines of many elements. G35–26 is of course too faint for the *IUE* but perhaps the *HST* could be used to measure the UV flux as well as the parallax. The appropriate resonance UV lines, that could be analyzed and used for abundance determinations in G35–26, lying above the steep changes in the flux at 1500 Å, include Mg I 2025, 2852 Å; Mg II 2795, 2802 Å; Ca I 2721 Å; Ca II 1650, 1652 Å; Si I 1770, 1841, 1988, 2516, 1697, 1850, 2216; Si II 1533, 1526, and 1816 Å. Some resonance lines of Al I are almost in the visible region and should be modeled and observed: 3961, 3944, and 3092 Å. An accurate parallax for G35–26 is particularly needed. It could be used to place an independent limit on the radius, and thus the mass, of G35–26. In order of importance, this is how we would list the things that need to be done to further the study of G35–26: Get a good spectrum for G35–26 (S/N $\sim$ 50 or more, but a lower S/N would be acceptable if the spectrum was free of ripples and bumps), measure the parallax accurately ($\delta\pi/\pi \sim 0.25$ or less), calculate effects of stratification and other convection theories, and consider the possibility that G35–26 is a binary system (see Liebert 1983).

The referee of this paper raised the objection that the broad Balmer lines—and here we use the phrase "broad" to mean wide and shallow—might be explainable by other means than high gravity. The idea would be that at lower temperature and a higher He/H ratio the importance of neutral perturbers increases, thus producing, through van der Waals broadening, the same line profile as high gravity. We tested this idea by performing model calculations at 10,000 K/log (g) = 8/(C/He) = 200 times solar with He/H = 400 and 800. The effect was to make the Balmer lines smaller, not broader. The lines remained quite narrow and pointy, quite the opposite to the appearance in the observed spectra. The referee's point is a good one, however, and when better data are available, such considerations should be made.

It is with pleasure that the authors acknowledge support from various sources: NASA grant NAG 5-972, NSF grant AST-8720530, and the Danish Research Academy, grant 880070. We also want to thank Stéphane Vennes and Detlev Koester for many interesting and important suggestions.

REFERENCES

Allen, C. W. 1973, *Astrophysical Quantities* (3d ed.; London: Athlone).
Auer, L. H. 1987, in *Numerical Radiative Transfer*, ed. W. Kalkofen (Cambridge: Cambridge University Press), p. 101.
Barnard, A. J., Cooper, J., and Shamey, L. J. 1969, *Astr. Ap.*, **1**, 28.
Bell, K. L., Hibbert, A., and Berrington, K. A. 1988, *J. Phys. B: At. Mol. Opt. Phys.*, **21**, 2319.
Dimitrijevic, M. S., and Popovic, M. M. 1989, *Astr. Ap.*, **217**, 201.
Fawcett, B. C. 1987, *Atomic Data Nucl. Data Tables*, **37**, 411.
Fontaine, G., Villeneuve, B., Wesemael, F., and Wegner, G. 1984, *Ap. J. (Letters)*, **277**, L61.
Goly, A., Rakotoarijimy, D., and Weniger, S. 1983, *J. Quant. Spectrosc. Rad. Transf.*, **30**, 417.
Gray, D. F. 1976, *The Observation and Analysis of Stellar Photospheres* (New York: John Wiley and Sons).

Greenstein, J. L. 1978, *Pub. A.S.P.*, **90**, 303.
Griem, H. R. 1974, in *Spectral Line Broadening by Plasmas*, ed. H. Massey and G. Brueckner (New York: Academic).
Hintzen, P., and Jensen, E. 1979, *Pub. A.S.P.*, **91**, 492.
Iben, I. 1984, in *IAU Symposium 105, Observational Tests of Stellar Evolution Theory*, ed. A. Maeder and A. Renzini (Dordrecht: Reidel), p. 3.
Kawai, Y., Saio, H., and Nomoto, K. 1988, *Ap. J.*, **328**, 207.
Kidder, K., Holberg, J. B., and Wesemael, F. 1988, in *IAU Colloquium 114, White Dwarfs*, ed. G. Wegner (New York: Springer), p. 350.
Koester, D., and Schönberner, D. 1986. *Astr. Ap.*, **154**, 125.
Koester, D., Weidemann, V., and Zeidler-K. T., E.-M. 1982 *Astr. Ap.*, **116**, 147.
Kurucz, R. 1970, *ATLAS: A Computer Program for Calculating Model Stellar Atmospheres* (*Smithsonian Ap. Obs. Spec. Rept.*, No. 309).
Liebert, J. 1983, *Pub. A.S.P.*, **95**, 878.
MacDonald, J., and Vennes, S. 1990, *Ap. J.*, submitted.
McCook, G. P., and Sion, E. M. 1987, *Ap. J. Suppl.*, **65**, 603.
Moore, C. E. 1971, *Atomic Energy Levels* (NSRDS-NBS 35) (Washington: National Bureau of Standards).
Myerscough, V. P., and McDowell, M. R. C. 1966, *M.N.R.A.S.*, **132**, 457.
Ng, K. C. 1974, *J. Chem. Phys.*, **61**, 2680.
Nomoto, K. 1984, *Ap. J.*, **277**, 791.
Pelletier, C., Fontaine, G., Wesemael, F., Michaud, G., and Wegner, G. 1986. *Ap. J.*, **307**, 242.
Sion, E. M., Fritz, M. L., McMullin, J. P., and Lallo, M. D. 1988, *A.J.*, **96**, 251.
Tarafdar, S. P., and Vardya, M. S. 1969, *M.N.R.A.S.*, **145**, 171.
Thejll, P. A., and Shipman, H. L. 1986, *Pub. A.S.P.*, **98**, 922.
Vauclair, G., and Fontaine, G. 1979. *Ap. J.*, **230**, 563.
Victor, G. A., and Escalante, V. 1988, *Atomic Data Nucl. Data Tables*, **40**, 203.
Wegner, G., and Koester, D. 1985, *Ap. J.*, **288**, 746.
Wegner, G., and Yackovich, F. H. 1983, *Ap. J.*, **275**, 240.
Wiese, W. L., and Konjevic, N. 1982, *J. Quant. Spectrosc. Rad. Transf.*, **28**, 185.
Wiese, W. L., Smith, M. W., and Glennon, B. M. 1966, *Atomic Transition Probabilities* (NSRDS-NBS 4) (Washington: National Bureau of Standards).
Yackovich, F. H. 1982, Ph.D. thesis, Pennsylvania State University.

JAMES MACDONALD, WILLIAM MACFARLAND, HARRY L. SHIPMAN, and PETER THEJLL: Department of Physics and Astronomy, University of Delaware, Newark, DE 19716